Microchimica Acta (2020) 187: 587
https://doi.org/10.1007/s00604-020-04451-z

ORIGINAL PAPER

Hydroquinone colorimetric sensing based on platinum deposited on CdS nanorods as peroxidase mimics

Xin Zhao[1] · Haoyuan Lyu[1] · Xiuxiu Yao[1] · Chang Xu[1] · Qingyun Liu[1] · Zhenxue Liu[1] · Xianxi Zhang[2] · Xiao Zhang[3]

Received: 6 February 2020 / Accepted: 12 July 2020 / Published online: 1 October 2020

Abstract

Pt deposited on CdS nanorods (Pt/CdS) have been prepared via the UV light photoreduction method. The Pt/CdS nanocomposites possess highly significant peroxidase-like activity with the assistance of the colorless substrate 3,3,5,5-tetramethylbenzidine (TMB). In the presence of peroxidase mimic Pt/CdS, TMB is quickly oxidized into a typical blue product (oxTMB, which has an obvious absorption at 652 nm) by H_2O_2 only in 3 min, which is easily detected visually. The catalytic activity of Pt/CdS originates from the accelerated electron transfer between the reactants. Combining the peroxidase-like activity of Pt/CdS with the blue change of TMB, a fast colorimetric sensing platform for detection of H_2O_2 has been constructed with a linear range 0.10–1.00 mM and a detection limit of 45.5 μM. The platform developed is further used to detect hydroquinone (HQ) in the range1.0–10 μM with a lower detection limit of 0.165 μM. The colorimetric platform has a potential to detect HQ residue in real water samples with recoveries ranging from 83.56 to 91.76%.

Keywords Pt/CdS · Peroxidase · H_2O_2 · Colorimetric detection · Hydroquinone

Introduction

Hydroquinone (HQ), as an important chemical intermediate and raw material, has been widely used in industrial production. Moreover, the isomer of HQ, catechol (CC), is also an important chemical raw material. HQ and its isomer often coexist in industrial sewage [1, 2]. According to the report, when the human body is exposed to acute high level of hydroquinone that will affect the central nervous system, resulting in tremor, convulsions, and death [3]. Therefore, it is of great practical significance to achieve the rapid and sensitive detection of HQ in water. Currently, the detection methods of HQ have been developed, including chromatography [4], colorimetry [5], and spectrophotometry [6]. Among them, the colorimetric method has been focused, because the detection results can be easily distinguished visually without expensive or sophisticated instruments.

As is well known, the challenge of colorimetric sensing is appropriate nanoenzymes to catalyze the oxidation of some organic substrates accompanied by a color change. In the past decades, scientists have developed various nanoperoxidase mimics, including noble metals [7], ferrite [8], and oxides [9]. As we know, nanocomposites usually exhibit developed performance, due to the synergetic effect from different components [10–14]. Therefore, scientists have focused on nanocomposites with the enhanced peroxidase-like activity, such as Co_3O_4-MMT NCs [9], and Au/Co_3O_4-CeOx NCs [7], due to the synergistic effect from different components in nanocomposites.

Pt, as one of precious metals, similar to Ru, Au, and Pd, has lower Fermi level and higher work function that can induce electrons to transfer from the surface of catalysts to

Electronic supplementary material The online version of this article (https://doi.org/10.1007/s00604-020-04451-z) contains supplementary material, which is available to authorized users.

✉ Qingyun Liu
qyliu@sdust.edu.cn

[1] College of Chemical and Biological Engineering, Shandong University of Science and Technology, Qingdao 266590, People's Republic of China

[2] Shandong Provincial Key Laboratory/Collaborative Innovation Center of Chemical Energy Storage & Novel Cell Technology, School of Chemistry and Chemical Engineering, Liaocheng University, Liaocheng 252059, People's Republic of China

[3] Shandong Key Laboratory of Biochemical Analysis, College of Chemistry and Molecular Engineering, Qingdao University of Science and Technology, Qingdao 266042, People's Republic of China

precious metals, facilitating the separation of charge carrier [15]. Nevertheless, the practical application of Pt nanoparticles is restricted, due to its disadvantages, such as easy aggregation, expensiveness, and easy poisoning. Thus, it is necessary to employ some good supports to disperse Pt nanoparticles to develop its catalytic activity, such as Pt@mSiO$_2$-NH$_2$ NPs [16] and Pt/Pt-Fe$_2$O$_3$NPs [15]. Notably, cadmium sulfide (CdS) nanomaterials have a potential application in biomedicine and biosensors, owing to their good photoluminescence properties, tunable band gap, and chemical stability [17]. Especially, CdS semiconductor nanoparticles have attracted intense interest in recent years in the treatment of the dye-polluted wastewater under visible light [18]. CdS has been often used for photocatalysis because its electronic structures match well with the redox potential of splitting water into hydrogen and oxygen molecules [19]. These studies suggest that the semiconductivity of CdS nanostructures plays an important role in catalytic reactions. Thus, if we combine CdS nanorods with noble Pt, the obtained Pt/CdS will benefit the electron transfer between substrates and reactants and then develop the catalytic activity of Pt/CdS nanocomposites.

Herein, platinum nanoparticles were deposited on CdS nanorods with the aid of irradiation of UV light, according to the previous publication [20]. In the preparation process, alcohol as an important electron donor was added in reaction system. Compared with pure CdS nanorods, Pt/CdS nanorods as excellent peroxidase mimics exhibited the superior catalytic activity. Base on the wonderful catalytic activity of Pt/CdS peroxidase mimics, a colorimetric method is constructed to detect H_2O_2 and HQ. The electrochemical results together with fluorescent data verified that the catalytic mechanism is from rapid transfer of electrons between the substrate TMB and H_2O_2 with the assistance of Pt/CdS nanorods.

Experimental sections

Materials

$Cd(NO_3)_2{}^{\bullet}4H_2O$, $CS(NH_2)_2$, 1,2-ethylenediamine (en), K_2PtCl_4, ethanol, hydroquinone, H_2O_2 (30 wt%), hydroquinone, fructose, sucrose, and various metal salts were purchased from Sinopharm Chemical Reagent Co. (Shanghai, China). DL-ISOLeucine (ISO), L-cysteine, D-histidine (His), urio acid (UA), L-arginine (Arg), DL-tryptophan (Try), and D-serine (Ser) were obtained from Sigma-Aldrich Co. LLC. 3,3,5,5-Tetramethylbenzidine (TMB) was purchased from Shanghai Macklin Biochemical Technology Co., Ltd.

Characterization

The as-prepared Pt/CdS nanorods are characterized by X-ray diffraction (D/Max 2500 PC, Rigaku) and transmission electron microscopy (TEM, JEOL, Japan) equipped with energy dispersive X-ray spectroscopy (EDX). The composition of Pt/CdS nanocomposites is detected by inductively coupled plasma atomic emission spectroscopy (ICP-AES, IRIS Intrepid II XRP, Shanghai) and X-ray photoelectron spectroscopy (XPS, Thermo, USA), respectively. The UV-1810 spectrophotometer (Shanghai, China) is used to measure the UV-vis absorption spectra, and the fluorescent spectra are recorded on F-4600 FLSPECTROPHOTOMET spectrofluorophotometer (Tokyo, Japan).

Preparation of CdS and Pt/CdS

The detailed preparation of CdS and Pt/CdS nanocomposites is presented in supporting information.

Assay of the peroxidase-like activity and steady-state kinetic of Pt/CdS

In the presence of H_2O_2, Pt/CdS as a peroxidase mimic can catalyze to oxidize TMB into ox-TMB. What is more, the color change could detect by UV-vis spectrophotometer through the absorbance signal change.

Similarly, the steady-state kinetic assays were implemented on foregoing reaction systems, which monitored the absorbance variation at 652 nm by a time-scan mode under the optimal condition ($T = 45$ °C, pH = 4.0). In the process of reactions, one substrate concentration was kept constant and varied another. The kinetics data were calculated according to the typical the Michaelis-Menten equation and double-reciprocal Lineweaver-Burk plot: $1/v = Km/V\max(1/[S] + 1/Km)$ [21], where v is the original velocity, Km is the Michaelis-Menten constant, Vmax is the maximal velocity of reaction, and [S] is the concentration of the substrate.

Colorimetric detection of hydroquinone

A series of experiments were carried out as follows: The mixed solution containing 1.2 mL HAc-NaAc buffer, 200 μL of H_2O_2, 200 μL of Pt/CdS nanorods (2 mg dissolved in 10 mL DI water), and 200 μL of TMB (0.3 mM) was incubated for 5 min at optimal temperature and was tested the absorbance (A_1). Immediately, 200 μL HQ with different concentration was added into the above mixture, and the absorbance was assigned as A_2. Thus, it is obtained the relationship of $\triangle A$ ($\triangle A = A_1 - A_2$) and the concentration of HQ.

Active species capturing

The hydroxyl radicals (•OH), superoxide radicals ($•O_2^-$), and holes (h^+) were captured by sacrificial agents, including IPA (2-propanol), PBQ (p-benzoquinone), and EDTA (disodium ethylene diamine tetraacetic acid).Similar to the experiment of detect hydrogen peroxide, above-mentioned sacrificial agents were added to the reaction systems before to add H_2O_2. The mixed solution containing 1.2 mL HAc-NaAc buffer, 200 μL of Pt/CdS nanorods (2 mg dissolved in 10 mL DI water), 200 μL of sacrificial agents, 200 μL of H_2O_2, and 200 μL of TMB (0.1 mM) was incubated for 5 min at optimal temperature and tested the absorbance A. While A_0 measured by using 200 μL HAc-NaAc buffer instead of sacrificial agents and set the value of A_0 as 100%, in order to facilitate the comparison with the measured A adding different sacrificial agents.

Detection of HQ in real sample

The real samples of lake water and river water were diluted using ultrapure water. HQ with different contents was spiked into these real water samples, guaranteeing that the final concentration of HQ was in the linear range. The mixture of 1.2 mL of acetate buffer, TMB (0.3 mM), H_2O_2 (25 mM), and Pt/CdS (0.2 mg/mL) was incubated for 5 min. Immediately, HQ solutions with different concentrations were added into the above mixture. The result was then analyzed using the rule of standard additions method [5], and the corresponding recoveries were inferred.

Results and discussion

Characterization of the nanocomposites

As shown in Fig. S1 (Supporting information), the diffraction peaks (2θ) at 28.182°, 24.807°, 26.502°, 36.602°, 43.681°, 47.839°, 51.824°, 58.278°, 66.772°, and 83.252° are in good agreement with the crystal planes (101), (100), (002), (102), (110), (103), (112), (202), (203), and (213) of hexagonal phase of CdS (JCPDS 41-1049). Obviously, the XRD data of CdS (A) are similar to that of Pt/CdS (B), suggesting that the crystal form of CdS in Pt/CdS is not changed. Unfortunately, the XRD diffraction peaks of Pt are not found in that of Pt/CdS, indicating that Pt nanoparticles are too small to be detected. It is further indicated that there is no change in crystallinity before and after platinum deposition.

Figure 1a and b show the SEM and TEM images of Pt/CdS, respectively. It is found that the rod-like morphology of Pt/CdS with the width range from 20 to 70 nm. From HRTEM image of Pt/CdS nanorods shown in Fig. 1c, it can be calculated that the distance of lattice planes is 0.320 nm, corresponding to the (101) plane of Pt/CdS nanorods. From EDX mapping images, Cd, S, and Pt elements are detected in the Pt/CdS nanorods (Fig. 1d).

ICP-MS is used to determine the elemental compositions of Pt/CdS nanorods. The result shows that the content of Pt and Cd in Pt/CdS nanorods is 1.245% and 97.941%, respectively. It is suggested that the content of Pt in the composites is very little. As we know, noble Pt is an expensive metal. In order to reduce the cost and save sources, the small amount of Pt in the nanocomposites should be controlled.

XPS is a powerful tool to examine the elements and chemical states. Figure S2 (Supporting information) shows the high-resolution core level spectra of Cd, S, and Pt elements. From Fig. S2A and S2B, the binding energy of Cd-$3d_{5/2}$, Cd-$3d_{3/2}$, S-$2p_{3/2}$, and S-$2p_{1/2}$ in the pure CdS is observed at 404.8, 411.6 and 161.34, and 162.4 eV, respectively, suggesting that Cd element is in + 2 state and S is in S^{2-} state. This is slightly different from the binding energy of Cd and S reported in the literature [22]. These results indicate that the transfer of electrons from CdS to Pt happens after platinum ions were reduced. The high-resolution spectrum of Pt 4f peak can be disassembled into three pair of peaks (Fig. S2C). Among which, the weak peak at around 67.8 eV is corresponding to Pt^0 $4f_{7/2}$. The other two strong peaks located at 72.4 eV and 75.7 eV are attributed to Pt^{2+} $4f_{7/2}$ and Pt^{2+} $4f_{5/2}$, respectively, revealing the existence of Pt^{2+} [23].

Influences of pH and temperatures

The following parameters were optimized: (a) Sample pH value is 4.0 and (b) temperature is 45 °C. Respective text and figures on optimizations are given in the Electronic Supporting Material.

Peroxidase-like activity of Pt/CdS

To investigate the peroxidase-like activity of Pt/CdS, six different reaction systems are designed. Figure 2 displays the absorbance and the corresponding photographs of different systems reacted for 3 min. From Fig. 2A, compared with that of the blank (sample a), the weak absorbance of system b with the negligible color change is found, indicating that H_2O_2 can slowly oxidize TMB into oxTMB. The curve c is the absorbance of CdS nanorods, corresponding to the pale yellow color shown in the inset. From the curve d together with the corresponding photograph, it can be found that Pt/CdS exhibits a weak oxidase-like activity. As displayed in curves e and f, the absorption intensity of sample f is much stronger than that of sample e, suggesting that Pt/CdS possesses a higher peroxidase-like activity than that of CdS, due to the introduction of Pt. This is further seen by the corresponding color change in the inset of photograph.

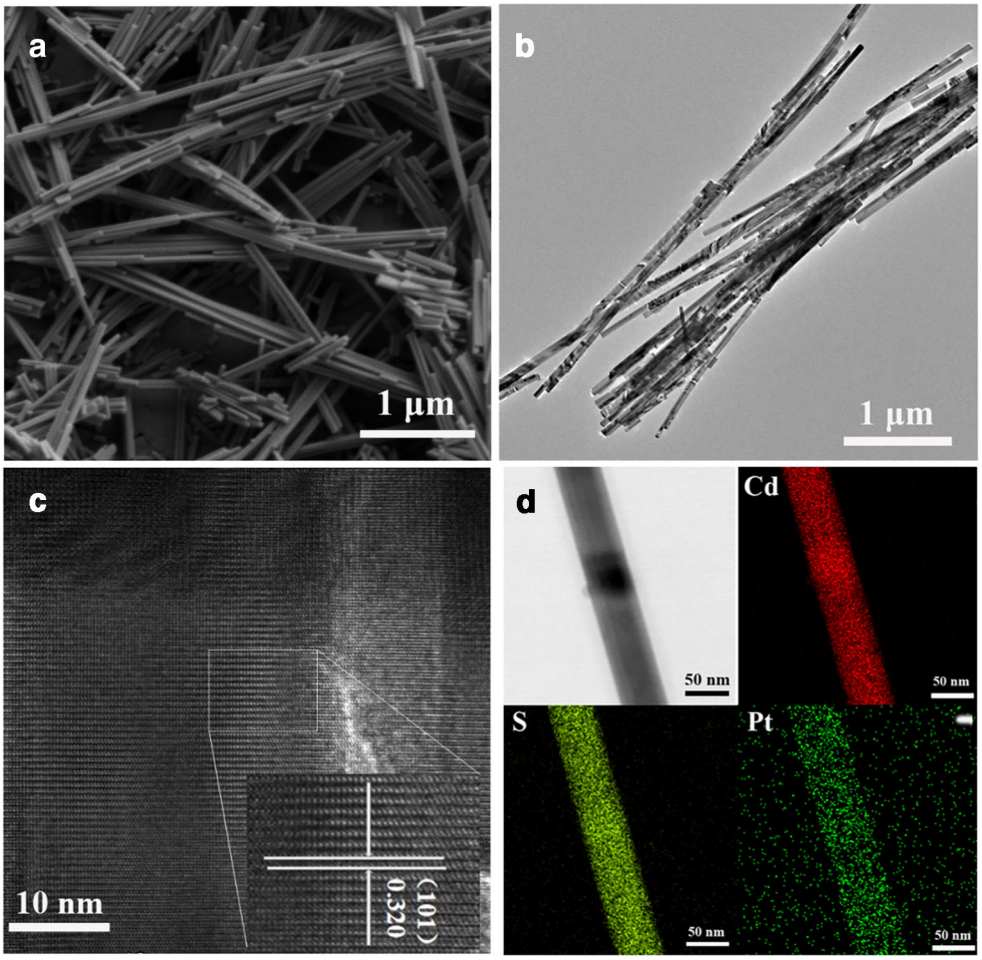

Fig. 1 SEM images of Pt/CdS (**a**), SEM images of Pt/CdS (**b**), the high-resolution TEM (HRTEM) image of Pt/CdS (**c**), and EDX mapping images of Cd, S, and Pt elements (**d**), respectively

Catalytic kinetics of Pt/CdS as peroxidase mimics

From the data shown in Fig. 3, it is well demonstrated that the peroxidase catalytic behaviors conform to the Michaelis-Menten model. Briefly, a higher K_m value means a poorer affinity between the substrate and peroxidase mimics. In comparison with some reported peroxidase-like performance, the related data have been summarized (Table S1). Compared with that of HRP [24], and artificial peroxidases, including AuNPs/PVP–GNs [25] and Fe_3O_4@Pt [26], the K_m of Pt/

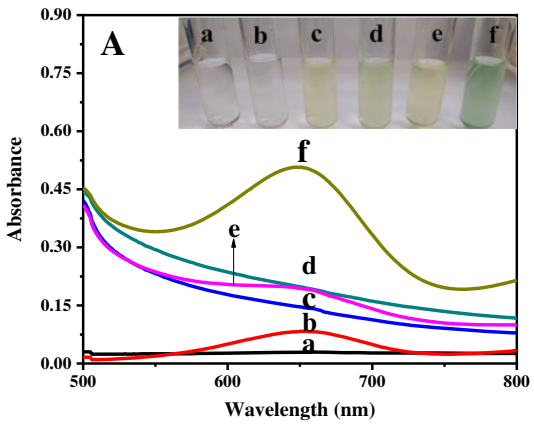

Systems	a	b	c	d	e	f
CdS	-	-	√	-	√	-
CdS/Pt	-	-	-	√	-	√
H_2O_2	-	√	-	-	√	√
TMB	√	√	√	√	√	√

Fig. 2 The absorbance change with wavelength from 500 nm to 800 nm of different reaction systems (response time 5 min). The inset of photograph is corresponding to the different experimental system's color variation. The panel labels shows all the things contained in the reaction system, where "√" represents existence, "-" represents non-existence. All these systems were incubated in optimal reaction conditions (pH 4 and temperature 45 C)

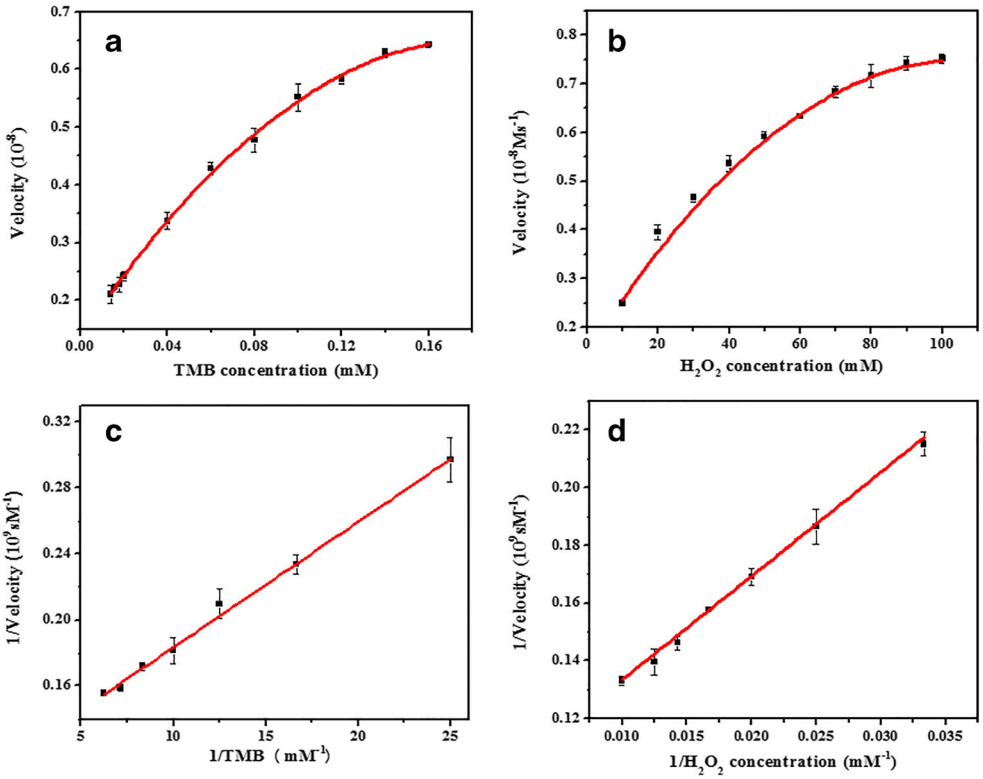

Fig. 3 Steady-state kinetic assay of Pt/CdS nanorods. **a** The concentration of H_2O_2 is 0.25 M, and the TMB concentration is varied. **b** The concentration of TMB is 1 mM, and the H_2O_2 concentration is varied. **c**, **d** Double reciprocal plots of the Michaelis-Menten equation from the activity date of the concentration of TMB and H_2O_2

CdS nanorods using TMB as the substrate is much lower, indicating that the affinity between TMB and Pt/CdS nanorods is stronger. In other words, the maximum activity of Pt/CdS nanorods is realized at a lower TMB concentration.

Determination of hydrogen peroxide

Figure 4a shows the response curve related the absorbance at 652 nm to the concentration of H_2O_2 from 1 to 10 mM. From Fig. 4a, it can be obtained the linear calibration plot of H_2O_2 from 100 to 1000 μM with the determination limit of 45.5 μM ($S/N = 3$). Compared with the previous studies listed in Table 1, it can be concluded that our fabricated sensing platform has a broader range than that based on PtCNPs [30], MoS_2-PtAg [31], and MOF(Co/2Fe) [32].

Determination platform of hydroquinone

Base on the peroxidase-like performance of Pt/CdS nanorods, a convenient colorimetric platform is constructed for determination of HQ. From Fig. 4b, it can be found that there is a linear relationship of ΔA ($\Delta A = A_1 - A_2$) and concentration of HQ. The correction equation is $\Delta Abs = 0.02545[HQ] + 0.10164$ ($R^2 = 0.99024$), displayed in Fig. 4b. Consequently, HQ is detected as low as 0.165 μM with a linear range from 1 to 10 μM. In order to compare the sensitivity of different methods for determination of HQ, we summarize the linear range and LOD of HQ obtained from the different method based on different peroxidase mimics, listed in Table S2. Clearly, the colorimetric platform based on Pt/CdS has a lower determination limit than that of AuNPs (1.6 μM) [27]. Notably, the determination limit of HQ is even lower than that electrochemistry based on Ni/N-MWCNT (11 nM) [28], which is famous for high sensitivity with the low determination limit. It is indicated that our colorimetric method exhibits a much high sensitivity. However, compared with most other electrochemistry methods [28, 29], the sensitivity of the colorimetric method is certain limitations.

Selectivity of the colorimetric sensor for detecting HQ

To verify the selectivity of the colorimetric determination for HQ, a series of control experiments are implemented using HQ; other phenols (e.g., phenol, resorcinol) and organic compounds containing phenolic groups (e.g., p-nitrophenol) have to be used for selectivity control and other potential interferents, such as HQ, Res, p-Nit, phOH, UA, Ser, His, Try, Arg, Iso, Cu^{2+}, Fe^{3+}, Suc, and Fru. The concentration of HQ is 5 μM, while that of other interferents is 50 μM. As shown in Fig. 4c, it can be obviously seen that the absorbance intensity of HQ is much stronger than that of interferents, even if the concentration of HQ is only one-tenth of interferents. It indicated the good selectivity of the colorimetric sensor for detecting HQ in the absence of the interfering reducing regents.

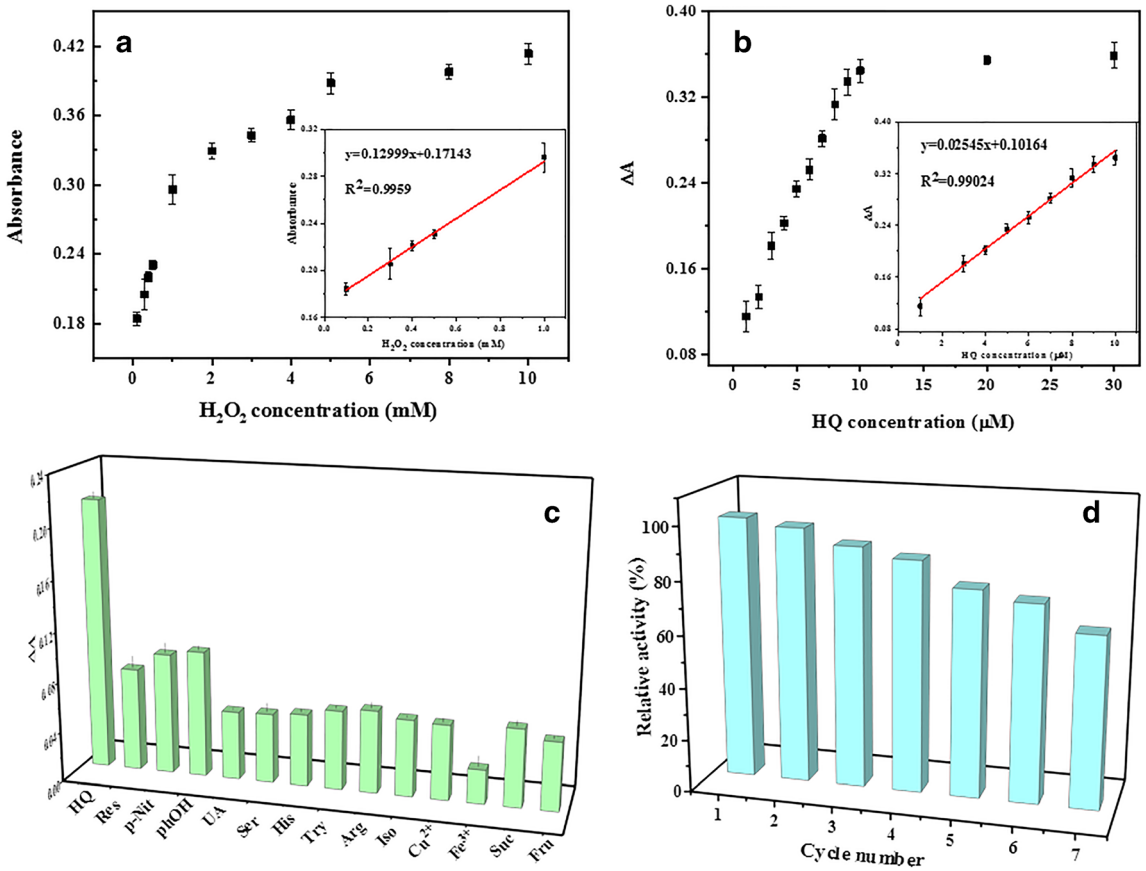

Fig. 4 **a** A dose-response curve depending of the absorbance at 652 nm on the concentration of H_2O_2 from 1 to 10 mM. Insert is the corresponding linear calibration plot of H_2O_2. **b** A dose-response curve depending of the absorbance at 652 nm on the concentration of HQ from 1 to 30 μM, and insert is the corresponding linear calibration plot of HQ, **c** the selectivity of determination of HQ, and **d** the reusability of catalytic CdS/Pt nanorods, respectively

Reusability of Pt/CdS nanorobs

As displayed in Fig. 4d, the relative activity of Pt/CdS remains more than 70% after being reacted for 7 cycles. A slight decrease of the peroxidase activity may be attributed to the loss during each centrifugation, indicating the pretty good reusability of Pt/CdS.

Catalytic mechanism of Pt/CdS

The peroxidase-like catalytic activity of the Pt/CdS is whether the electron transfer between TMB and H_2O_2 occurs. In order to verify the hypothesis, we explore the electrocatalytic behaviors of Pt/CdS toward the electrochemical reduction of H_2O_2 by using amperometric responses and cyclic voltammetry in standard conditions. As can be seen for Fig. 5, there is no obvious current in the absence of H_2O_2, while an obvious current occurs in the presence of H_2O_2. Compared with the electrocatalytic behavior of bare GCE with Pt/CdS modified GCE, as shown in Fig. 5B, there is no obvious current for bare GCE, while an obvious reduction current increases steeply to reach a steady-state value with addition of an aliquot of H_2O_2 for Pt/CdS modified GCE. It is suggested that Pt/CdS possesses an electrocatalytic activity of reduction of H_2O_2 by accelerating electron transfer between H_2O_2 (electron acceptor) and GCE (electron donor). Similarly, it is concluded that Pt/CdS can also accelerate the electron transfer between H_2O_2 and TMB. In this process, TMB as an electron contributor is

Table 1 Comparison of the linear range and the limit of determination of HQ by different determination methods

Materials	Detected substance	Analytical methods	Linear range	LOD	References
Pt/CdS	Hydroquinone	Colorimetry	1–10 μM	0.165 μM	This work
AuNPs	Hydroquinone	Colorimetry	2.7–19 μM	1.6 μM	[27]
Ni/N-MWCNT	Hydroquinone	Electrochemistry	0.3–300 μM	11 nM	[28]
HMCCSs	Hydroquinone	Electrochemistry	0.3~1000 μM	0.12 μM	[29]

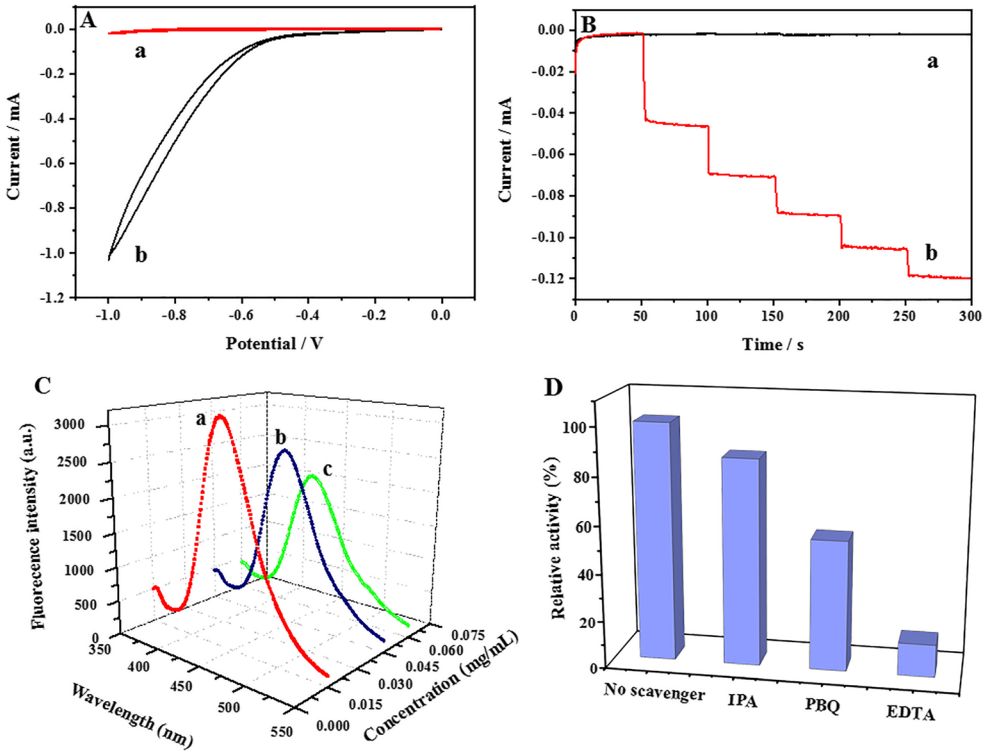

Fig. 5 (A) Cyclic voltammograms of the Pt/CdS nanorods modified GCE electrode in the absence (a) and in the presence of 100 mM H_2O_2 (b). Scan rate, 50 mV s^{-1}. (B) Amperometric response of bare GCE (a) and the Pt/CdS nanorods modified GCE (b) at applied potential of 0.6 V upon successive additions of 1 mM H_2O_2 50 μL. All systems were incubated in 100 mM phosphate buffer saline (PBS) plus 100 mM KCl (pH 5.7). (C) The effect of the concentration of NiS/MMT/GO on electron transfer with terephthalic acid as fluorescent probe. Experimental conditions: TA (0.5 mM), H_2O_2 (25 mM), and the Pt/CdS nanorods with different concentration (a–c: 0.015, 0.045, 0.06 mg·mL^{-1}) were cultivated in acetate buffer (pH = 4.0) at 45 °C for 30 min. (D) Capture assays of active species during the catalysis of TMB over CdS/Pt nanorods

donated lone-pair electrons from the amino groups to the Pt/CdS [33], resulting in increasing of electron density and mobility in the surface of Pt/CdS. This would accelerate the electron transfer from the Pt/CdS to H_2O_2 [34]. Thus, the oxidation of TMB by H_2O_2 is dramatically developed after the addition of Pt/CdS. With CdS excited by visible light, photo-induced electrons in the conduction band of CdS nanorobs can transfer easily into Pt through the Schottky barrier, because the Fermi level of CdS is higher than that of the deposited Pt [35]. The introduction of Pt hindered the

Scheme 1 Schematic illustration of the colorimetric determination of HQ

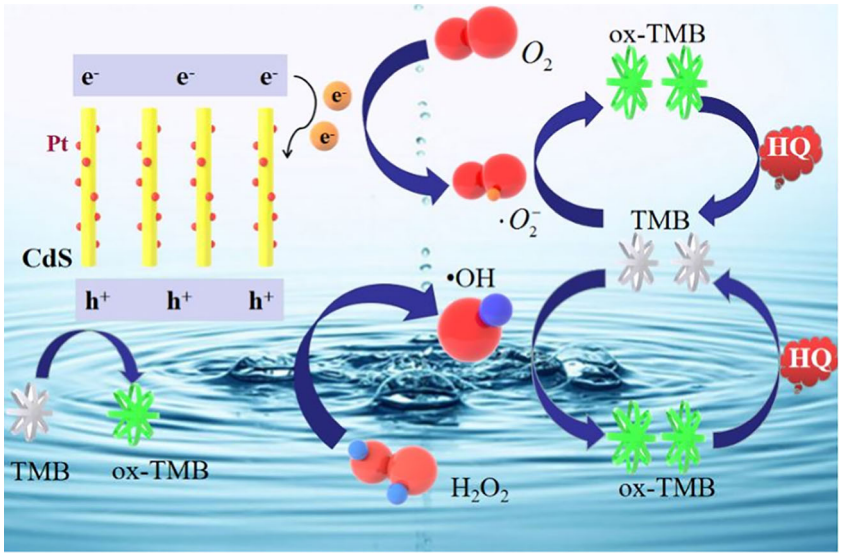

Table 2 The recoveries of hydroquinone standard solution in water samples using the colorimetric system

Sample	Added (μM)	Found (μM)	Recovery (%)	RSD (%, $n = 4$)
Lake water	6	5.014	83.56	1.390
	4	3.538	88.45	1.163
River water	8	6.871	85.88	0.6399
	6	5.505	91.76	0.8237
	4	3.511	87.78	0.5781

electron-hole recombination of CdS. It accelerates the electron transfer from the Pt/CdS to H_2O_2.

According to the previous reports, the catalytic mechanisms of artificial peroxidases are classified into two kinds. One is the electron transfer between substrates and H_2O_2. The other is active species in catalytic systems. To investigate the possible mechanism of catalytic behaviors of Pt/CdS, two methods including fluorescence probe and electrochemistry are used in the work. Firstly, terephthalic acid/H_2O_2 system is chosen to examine whether the peroxidase-like activity of Pt/CdS is related to the generation of OH. Thus, the terephthalic acid, as a fluorescence probe, can yield a highly fluorescent product (2-hydroxy terephthalic acid) after reacting with OH. As shown in Fig. 5C, the intensity of fluorescence is gradually decreased with increasing of Pt/CdS, which is similar to that of Co_3O_4 nanoparticles while different from that of the H_2TCPP-NiO, indicating that the catalytic mechanism of Pt/CdS is not contribute to OH.

To explore active species in the Pt/CdS system, three radical scavengers containing IPA (2-propanol), PBQ (p-benzoquinone), and EDTA (disodium ethylene diamine tetraacetic acid) were used to capture •OH, $•O_2^-$, and h^+, respectively. From Fig. 5D, we can observe a distinct decrease of the relative activity of Pt/CdS when adding the EDTA and PBQ; it suggests that h^+ and $•O_2^-$ play a crucial role during the catalytic process. While along with the addition of IPA, the relative activity dropped slightly, meaning that bits of •OH working in the reaction.

The main reactions involved in the catalytic process were followed:

$$O_2 + e_{CB}^- \rightarrow •O_2^- \quad (1)$$

$$H_2O_2 + h_{VB}^+ \rightarrow 2•OH \quad (2)$$

$$•O_2^-, h_{VB}^+, •OH + TMB \rightarrow ox\ TMB \quad (3)$$

The catalytic mechanism of Pt/CdS as a peroxidase mimic is manifest in Scheme 1.

Determination of HQ in real samples

The applicable feasibility of the colorimetric method is applied in the determination of HQ in the lake and river water samples. A series of samples with different concentration of HQ are spiked into lake water and river water. The percentage recovery values are listed in Table 2. The recoveries for HQ determined for these spiked samples range from 83.56 to 91.76%. Each sample undergoes three parallels determination, and the RSD is below 1.390%, suggesting that the results obtained by this sensor are acceptable. The recoveries are calculated based on the equation of recovery (%) = found/added × 100.

Conclusions

In this work, Pt loaded on CdS nanorods are prepared by the photoreduction deposition method. Although the content of Pt in nanorods is very little, Pt/CdS exhibit the superior peroxidase-like performance, which follows the typical Michaelis-Menten theory. The catalytic mechanism of Pt/CdS is attributed to not only the fast electron transfer but also the produced active species ($•O_2^-$, h_{VB}^+, and •OH) in the catalytic system. Base on the superior peroxidase-like performance of Pt/CdS, a colorimetric sensing platform with high sensitivity and selectivity for H_2O_2 and HQ has been constructed and used to detect HQ in top water, lake water, and river water samples. The economic and environmental-friendly colorimetric platform has a great potential application in determination of environmental pollutants.

Funding Finance supports from the National Natural Science Foundation of China (Grant No. 21971152), Natural Science Foundation of Shandong Province (Grant No. ZR2018MB002 and ZR2018MEE003), the open fund of Qingdao University of Science and Technology (No. QUSTHX202001), and Innovation Fund of Science & Technology of Graduate Students (SDKDYC190216).

Compliance with ethical standards

Conflict of interest The authors declare that they have no conflict of interest.

References

1. Wang J, Park J-N, Wei X-Y, Lee CW (2003) Room-temperature heterogeneous hydroxylation of phenol with hydrogen peroxide over Fe^{2+}, Co^{2+} ion-exchanged Naβ zeolite. Chem Commun 5: 628–629. https://doi.org/10.1039/b212296k

2. Guo Q, Huang J, Chen P, Liu Y, Hou H, You T (2012) Simultaneous determination of catechol and hydroquinone using electrospun carbon nanofibers modified electrode. Sensor Actuat B-Chem 163(1):179–185. https://doi.org/10.1016/j.snb.2012.01.032
3. World Health Organization (1996) Hydroquinone health and safety guide. Geneva World Health Organization. https://apps.who.int/iris/bitstream/handle/10665/38140/924151101X-eng.pdf
4. Marrubini G, Calleri E, Coccini T, Castoldi AF, Manzo L (2005) Direct analysis of phenol, catechol and hydroquinone in human urine by coupled-column HPLC with fluorimetric detection. Chromatographia 62(1–2):25–31. https://doi.org/10.1365/s10337-005-0570-3
5. Yang H, Zha J, Zhang P, Qin Y, Chen T, Ye F (2017) Fabrication of $CeVO_4$ as nanozyme for facile colorimetric discrimination of hydroquinone from resorcinol and catechol. Sensor Actuat B-Chem 247:247469–247478. https://doi.org/10.1016/j.snb.2017.03.042
6. Nghia NN, Huy BT, Lee YI (2018) Colorimetric detection of chromium(VI) using graphene oxide nanoparticles acting as a peroxidase mimetic catalyst and 8-hydroxyquinoline as an inhibitor. Mikrochim Acta 186(1):36. https://doi.org/10.1007/s00604-018-3169-8
7. Liu H, Ding Y, Yang B, Liu Z, Liu Q, Zhang X (2018) Colorimetric and ultrasensitive detection of H_2O_2 based on Au/Co_3O_4 -CeOx nanocomposites with enhanced peroxidase-like performance. Sensor Actuat B-Chem 271:336–345. https://doi.org/10.1016/j.snb.2018.05.108
8. Lyu H, Zhao X, Yao X, Chen W, Liu Z, Gao L, Fan G, Zhu X, Liu Q, Zhang X, Zhang X (2020) 3,4:9,10-perylene tetracarboxylic acid-modified zinc ferrite with the enhanced peroxidase activity for sensing of ascorbic acid. Colloids Surfaces A 586:124250. https://doi.org/10.1016/j.colsurfa.2019.124250
9. Gao Y, Wu K, Li H, Chen W, Fu M, Yue K, Zhu X, Liu Q (2018) Glutathione detection based on peroxidase-like activity of Co_3O_4–Montmorillonite nanocomposites. Sensor Actuat B-Chem 273:1635–1639. https://doi.org/10.1016/j.snb.2018.07.091
10. Ghasemipour P, Fattahi M, Rasekh B, Yazdian F (2020) Developing the ternary ZnO doped MoS_2 nanostructures grafted on CNT and reduced graphene oxide (RGO) for photocatalytic degradation of aniline. Sci Rep 10(1):4414. https://doi.org/10.1038/s41598-020-61367-7
11. Payan A, Fattahi M, Roozbehani B (2018) Synthesis, characterization and evaluations of TiO_2 nanostructures prepared from different titania precursors for photocatalytic degradation of 4-chlorophenol in aqueous solution. J Environ Health Sci Eng 16(1):41–54. https://doi.org/10.1007/s40201-018-0295-5
12. Shojaie A, Fattahi M, Jorfi S, Ghasemi B (2018) Synthesis and evaluations of Fe_3O_4–TiO_2–Ag nanocomposites for photocatalytic degradation of 4-chlorophenol (4-CP): effect of Ag and Fe compositions. Int J Ind Chem 9(2):141–151. https://doi.org/10.1007/s40090-018-0145-4
13. Ashouri R, Ghasemipoor P, Rasekh B, Yazdian F, Mofradnia SR, fattahi M. (2018) The effect of ZnO-based carbonaceous materials for degradation of benzoic pollutants: a review. Int J Environ Sci Technol 16(3):1729–1740. https://doi.org/10.1007/s13762-018-2056-5
14. Hayati F, Isari AA, Anvaripour B, Fattahi M, Kakavandi B (2020) Ultrasound-assisted photocatalytic degradation of sulfadiazine using MgO@CNT heterojunction composite: effective factors, pathway and biodegradability studies. Chem Eng J 381:122636. https://doi.org/10.1016/j.cej.2019.122636
15. Liu H, Tian K, Ning J, Zhong Y, Zhang Z, Hu Y (2019) One-step solvothermal formation of Pt nanoparticles decorated Pt^{2+}-doped α-Fe_2O_3 nanoplates with enhanced photocatalytic O_2 evolution. ACS Catal 9(2):1211–1219. https://doi.org/10.1021/acscatal.8b03819
16. Wang Z, Yang X, Yang J, Jiang Y, He N (2015) Peroxidase-like activity of mesoporous silica encapsulated Pt nanoparticle and its application in colorimetric immunoassay. Anal Chim Acta 862:53–63. https://doi.org/10.1016/j.aca.2014.12.046
17. Padmaja S, Jayakumar S (2019) Tunable luminescence and transmittance nature of CdS:PMMA nanocomposites for optoelectronic applications. Opt Laser Technol 112:112409–112412. https://doi.org/10.1016/j.optlastec.2018.11.038
18. Liu Q, Zhu R, Jiang Y, Jia Q, Yang S, Shao Q, Wang D, Cui P (2014) The facile preparation of 5,10,15,20-tetrakis(4-carboxyl phenyl) porphyrin-CdS nanocomposites and their photocatalytic activity. Mater Sci Eng B 188:188106–188113. https://doi.org/10.1016/j.mseb.2014.05.002
19. Yin XL, Liu J, Jiang WJ, Zhang X, Hu JS, Wan LJ (2015) Urchin-like Au@CdS/WO_3 micro/nano heterostructure as a visible-light driven photocatalyst for efficient hydrogen generation. Chem Commun (Camb) 51(72):13842–13845. https://doi.org/10.1039/c5cc05211d
20. Kolobov NS, Svintsitskiy DA, Kozlova EA, Selishchev DS, Kozlov DV (2017) UV-LED photocatalytic oxidation of carbon monoxide over TiO_2 supported with noble metal nanoparticles. Chem Eng J 314:600–611. https://doi.org/10.1016/j.cej.2016.12.018
21. Ding Y, Liu H, Gao L-N, Fu M, Luo X, Zhang X, Liu Q, Zeng R-C (2019) Fe-doped Ag_2S with excellent peroxidase-like activity for colorimetric determination of H_2O_2. J Alloy Compd 785:1189–1197. https://doi.org/10.1016/j.jallcom.2019.01.225
22. Rama Krishna Chava JYD, Kang M (2018) Smart hybridization of Au coupled CdS nanorods with few layered MoS_2 nanosheets for high performance photocatalytic hydrogen evolution reaction. ACS Sustain Chem Eng. https://doi.org/10.1021/acssuschemeng.8b00249
23. Hanifah MFR, Jaafar J, Othman MHD, Ismail AF, Rahman MA, Yusof N, Aziz F, Rahman NAA (2019) One-pot synthesis of efficient reduced graphene oxide supported binary Pt-Pd alloy nanoparticles as superior electro-catalyst and its electro-catalytic performance toward methanol electro-oxidation reaction in direct methanol fuel cell. J Alloy Compd 793:232–246. https://doi.org/10.1016/j.jallcom.2019.04.114
24. Gao L, Zhuang J, Nie L, Zhang J, Zhang Y, Gu N, Wang T, Feng J, Yang D, Perrett S, Yan X (2007) Intrinsic peroxidase-like activity of ferromagnetic nanoparticles. Nat Nanotechnol 2(9):577–583. https://doi.org/10.1038/nnano.2007.260
25. Chen X, Tian X, Su B, Huang Z, Chen X, Oyama M (2014) Au nanoparticles on citrate-functionalized graphene nanosheets with a high peroxidase-like performance. Dalton Trans 43(20):7449–7454. https://doi.org/10.1039/c3dt53316f
26. Ma M, Xie J, Zhang Y, Chen Z, Gu N (2013) Fe_3O_4@Pt nanoparticles with enhanced peroxidase-like catalytic activity. Mater Lett 105:36–39. https://doi.org/10.1016/j.matlet.2013.04.020
27. Zhang L-p, Xing Y-p, Liu L-h, Zhou X-h, Shi H-c (2016) Fenton reaction-triggered colorimetric detection of phenols in water samples using unmodified gold nanoparticles. Sensor Actuat B-Chem 225:593–599. https://doi.org/10.1016/j.snb.2015.11.083
28. Rajkumar C, Thirumalraj B, Chen S-M, Veerakumar P, Lin K-C (2018) Voltammetric determination of catechol and hydroquinone using nitrogen-doped multiwalled carbon nanotubes modified with nickel nanoparticles. Microchim Acta 185(8). https://doi.org/10.1007/s00604-018-2926-z
29. Ren H, Zhang Y, Liu L, Li Y, Wang D, Zhang R, Zhang W, Li Y, Ye BC (2019) Synthesis of hollow Mo_2C/carbon spheres, and their application to simultaneous electrochemical detection of hydroquinone, catechol, and resorcinol. Microchim Acta 186(5):306. https://doi.org/10.1007/s00604-019-3432-7
30. Bao Y-W, Hua X-W, Ran H-H, Zeng J, Wu F-G (2019) Metal-doped carbon nanoparticles with intrinsic peroxidase-like activity

for colorimetric detection of H_2O_2 and glucose. J Mater Chem B 7(2):296–304. https://doi.org/10.1039/c8tb02404a

31. Cai S, Han Q, Qi C, Lian Z, Jia X, Yang R, Wang C (2016) Pt74Ag26 nanoparticle-decorated ultrathin MoS_2 nanosheets as novel peroxidase mimics for highly selective colorimetric detection of H_2O_2 and glucose. Nanoscale 8(6):3685–3693. https://doi.org/10.1039/c5nr08038j
32. Yang H, Yang R, Zhang P, Qin Y, Chen T, Ye F (2017) A bimetallic (Co/2Fe) metal-organic framework with oxidase and peroxidase mimicking activity for colorimetric detection of hydrogen peroxide. Microchim Acta 184(12):4629–4635. https://doi.org/10.1007/s00604-017-2509-4
33. Qin W, Su L, Yang C, Ma Y, Zhang H, Chen X (2014) Colorimetric detection of sulfite in foods by a TMB-O_2-Co_3O_4 nanoparticles detection system. J Agric Food Chem 62(25):5827–5834. https://doi.org/10.1021/jf500950p
34. Fattahi M, Kazemeini M, Khorasheh F, Rashidi A (2014) An investigation of the oxidative dehydrogenation of propane kinetics over a vanadium–graphene catalyst aiming at minimizing of the COx species. Chem Eng J 250:25014–25024. https://doi.org/10.1016/j.cej.2014.04.002
35. Barghi B, Fattahi M, Khorasheh F (2014) The modeling of kinetics and catalyst deactivation in propane dehydrogenation over Pt-Sn/γ-Al_2O_3in presence of water as an oxygenated additive. Petrol Sci Technol 32(10):1139–1149. https://doi.org/10.1080/10916466.2011.631071